Catalysis Today 149 (2010) 267–274

Contents lists available at ScienceDirect

Catalysis Today

journal homepage: www.elsevier.com/locate/cattod

Synthesis of ionones on solid Brønsted acid catalysts: Effect of acid site strength on ionone isomer selectivity

V.K. Díez *, C.R. Apesteguía, J.I. Di Cosimo

Catalysis Science and Engineering Research Group (GICIC), INCAPE, UNL-CONICET, Santiago del Estero 2654, 3000 Santa Fe, Argentina

ARTICLE INFO

Article history:
Available online 3 November 2009

Keywords:
Ionone isomers
Acid catalysis
Tungstophosphoric acid
Triflic acid

ABSTRACT

The effect of Brønsted acid site strength on the liquid-phase conversion of pseudoionone to ionone isomers (α-, β- and γ-ionone) was studied on resin Amberlyst 35W, silica-supported heteropolyacid (HPAS) and silica-supported triflic acid (TFAS). Catalyst acidity was probed by temperature-programmed desorption of NH_3 coupled with infrared spectra of adsorbed pyridine. The initial pseudoionone conversion rate followed the order: TFAS > Amberlyst 35W ≈ HPAS. Synthesis of the three ionone isomers occurred via a common cyclic carbocation intermediate formed from the activation of the pseudoionone molecule on Brønsted acid sites. Initial ionone mixtures containing a α:β:γ isomer distribution of about 40:20:40 were formed, irrespective of the acid site strength. But the ionone mixture composition changed with the progress of the reaction because γ-ionone was consecutively converted to α-ionone on HPAS and Amberlyst 35W, whereas the stronger acid sites of TFAS converted γ-ionone to β-ionone.

© 2009 Elsevier B.V. All rights reserved.

1. Introduction

Ionone isomers are fine chemicals widely used as pharmaceuticals and fragrances. Specifically, β-ionone is an important precursor in the synthesis of vitamin A whereas α- and γ-ionones are in high demand in the fragrance industry because of their violet and woody-fruity scent, respectively [1,2]. The current commercial synthesis of ionones from acetone and citral uses homogeneous catalysis and involves a two-step process, as illustrated in Scheme 1. Initially, the liquid-phase aldol condensation of citral with acetone is catalyzed by diluted bases and forms selectively pseudoionones. The consecutive cyclization of pseudoionones to yield ionone isomers is catalyzed by liquid acids [3], which entails environmental concerns because of corrosion and waste disposal. Then, new industrial strategies for ionone synthesis from pseudoionone cyclization demand the replacement of liquid acids by solid catalysts.

However, very few papers have been published on the use of solid acids for converting pseudoionone to ionone isomers. Lin et al. [4] reported that cationic ion-exchange resins convert pseudoionone to an ionone mixture containing α- and β-isomers; total ionone yields were between 20 and 40%. Similar values were reported by Guo et al. [5] employing sulfated and persulfated TiO_2/MCM-41. These ionone yields obtained on solid acids were significantly lower than those reported via the homogeneous reaction (70–90%). A better approach to the homogeneous catalyst performance was reached in our recent contributions [6,7], in which we explored the synthesis of ionones on several solid acids such as bulk tungstophosphoric acid (HPA), silica-supported HPA containing between 18.8 and 58.5% HPA, Cs-HPA, zeolite HBEA, SiO_2–Al_2O_3 and Amberlyst 35W resin. Results showed that the reaction can be efficiently promoted on catalysts containing a high density of strong Brønsted acid sites. The highest ionone yield, 79%, was obtained on a 58.5 wt.% HPA/SiO_2 catalyst at 383 K and is comparable to the best values reported in the literature for the homogeneously catalyzed reaction using sulfuric acid.

Here, our research specifically focuses on the effect of Brønsted acid site strength on ionone isomer selectivity. Previous work using homogeneous catalysts showed that the ionone isomer distribution depends on the nature, concentration and strength of the liquid acid catalyst. For example, it has been reported that concentrated sulfuric acid produces predominantly β-ionone [8,9] while phosphoric acid forms essentially α-ionone [3]. In contrast, γ-ionone is the main isomer when Lewis acids such as BF_3 are used [10]. To the best of our knowledge, there are not in the literature papers dealing with the effect of the acid site density and strength of solid catalysts on the ionone isomer selectivity. In this work, we prepared solid Brønsted acid catalysts, namely resin Amberlyst 35W, silica-supported heteropolyacid and silica-supported triflic acid, with the aim of correlating the catalyst acid site strength with the resulting ionone isomer distribution. Our results show that the relative concentration of α-, β- and γ-ionone in the ionone mixture

* Corresponding author. Tel.: +54 342 4555279; fax: +54 342 4531068.
E-mail address: verodiez@fiq.unl.edu.ar (V.K. Díez).

0920-5861/$ – see front matter © 2009 Elsevier B.V. All rights reserved.
doi:10.1016/j.cattod.2009.09.016

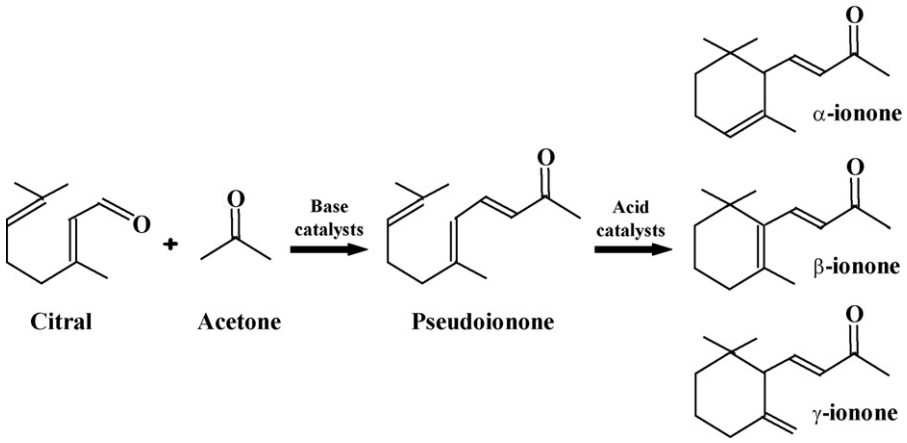

Scheme 1. Two-step process for ionone synthesis.

can be controlled by changing the catalyst Brønsted acid site strength and the operative conditions, in particular temperature and reaction time.

2. Experimental

2.1. Catalyst synthesis and activation

HPA/SiO_2 (HPAS) and TFA/SiO_2 (TFAS) catalysts with acid contents of 58.5 and 8.2 wt.%, respectively, were prepared by incipient wetness impregnation. Tungstophosphoric acid ($H_3PW_{12}O_{40}{\cdot}xH_2O$, Merck, GR) and triflic acid (CF_3SO_3H, Sigma–Aldrich, Reagent Grade) were added to a commercial SiO_2 (Grace Davison, G62, 99.7%, 272 m^2/g, pore diameter = 122 Å) using aqueous solutions of HPA and TFA. The impregnated samples were both dried at 353 K and then decomposed and stabilized at 523 K (HPAS) and 383 K (TFAS) for 18 h in N_2 (40 cm^3/min).

Amberlyst 35W resin pellets (Rohm and Haas) were crushed and sieved to retain particles between 180 and 480 μm. Then, the resin was treated in N_2 (40 cm^3/min) at 373 K overnight.

2.2. Catalyst characterization

The HPA content in HPAS catalyst was determined via the analysis of tungsten by UV spectroscopy in a Metrolab 1700 UV–vis spectrometer. Sample was calcined in an oven at 1073 K to transform $H_3PW_{12}O_{40}{\cdot}xH_2O$ in tungsten oxide (WO_3) and then digested in an alkali solution. The solution containing WO_3 was finally analyzed by UV–vis technique. The TFA loading in TFAS was determined by titration of sample protons. TFAS (0.3 g) was suspended in 75 ml of an aqueous solution of KCl (0.03 M) to release the triflic acid protons to the aqueous solution. The suspension was stirred for 20 min and then titrated with a 0.06 M KOH solution using phenolphthalein as acid–base indicator.

BET surface areas were measured by N_2 physisorption at its boiling point using an Autosorb Quantachrome 1-C sorptometer.

The acid site density (n_a) of HPAS catalyst was measured by temperature-programmed desorption (TPD) of NH_3 preadsorbed at 373 K. Sample (150 mg) was treated in He (40 cm^3/min) at 523 K for 1 h, cooled down to 373 K, and then exposed to a 1% NH_3/He stream during 15 min. Weakly adsorbed NH_3 was removed by flushing with He at 373 K during 1 h. Finally, the sample temperature was increased from 373 to 1073 K at a rate of 10 K/min in a He flow of 60 cm^3/min. Desorbed NH_3 was analyzed by mass spectrometry (MS) in a Baltzers Omnistar unit.

The chemical nature of surface acid sites on HPAS and TFAS catalysts was determined by Infrared Spectroscopy (IR) by using pyridine as probe molecule and a Shimadzu FTIR Prestige-21 spectrophotometer. Sample wafers were formed by pressing 20–40 mg of the catalyst at 5 ton/cm^2 and transferred to a sample holder made of quartz. An inverted T-shaped Pyrex cell containing the sample pellet was used. The two ends of the short arm of the T were fitted with CaF_2 windows. Sample wafers were evacuated 4 h at 523 K for HPAS and 353 K for TFAS and then the catalyst spectrum was recorded after cooling the sample at room temperature. After that, admission of 0.12 kPa of pyridine and adsorption at room temperature were performed, followed by sequential evacuation at 298, 373, 423 and 473 K for HPAS and 298 and 353 K for TFAS. Spectra were recorded at room temperature and the spectra of the adsorbed species were obtained by subtracting the catalyst spectrum.

2.3. Catalytic testing

The cyclization of pseudoionone (Fluka, >90%) was carried out at 353 K under autogenous pressure (≈250 kPa) in a batch PARR reactor, using toluene as aprotic solvent and a catalyst/PS = 28–56 wt.% ratio. Catalysts were pretreated ex situ in a N_2 stream at the calcination temperature for 2 h to remove adsorbed water. After introducing the reactant and solvent the reactor was sealed and flushed with N_2 and then the mixture was heated up to the final reaction temperature under stirring (300 rpm). Then the catalyst was added to the reaction mixture to start the reaction. Catalysts were loaded as ground powders in which inter- and intra-particle diffusional limitations were verified to be negligible. Reaction products were periodically analyzed during the 6-h reaction in a Varian Star 3400 CX gas chromatograph equipped with an FID and a Carbowax Amine 30 M capillary column. Main reaction products were ionones (α-, β- and γ-isomers). Selectivities (S_j, mol of product j/mol of PS reacted) were calculated as $S_j = C_j/\sum C_j$ where C_j is the concentration of product j. Product yields (η_j, mol of product j/mol of PS fed) were calculated as $\eta_j = S_j \times X_{PS}$, where X_{PS} is the pseudoionone conversion.

3. Results and discussion

3.1. Catalyst characterization

The surface areas and acid properties of the catalysts are presented in Table 1. Incorporation of bulky HPA species to SiO_2 caused a significant diminution of the SiO_2 surface area, from 272 to 144 m^2/g (HPAS sample), probably because of the formation of an incipient three-dimensional HPA structure that partially blocks the silica pores. The presence of the heteropolyacid structure in

Table 1
Surface area and acid properties of HPAS, TFAS and Amberlyst 35W samples.

Catalyst	Surface area (m^2/g)	Surface acid properties				
		Acid site density		Acid site nature by FTIR		
		n_a[a] (μmol/g)	n_{H+} (μmol/g)	*B* (area/g)	*L* (area/g)	*B*/(*B*+*L*) (%)
TFAS	245	–	540[b]	222[c]	18[c]	93
Amberlyst 35W	39	–	5200[d]	–	–	–
HPAS	144	566	610[e]	450[f]	56[f]	89

B: Brønsted sites, *L*: Lewis sites.
[a] By TPD of NH_3.
[b] By acid–base titration.
[c] Data obtained after pyridine admission at 298 K and evacuation at 353 K.
[d] From manufacturer information.
[e] By UV spectroscopy analysis.
[f] Data obtained after pyridine admission at 298 K and evacuation at 373 K.

HPAS sample after impregnation and calcination was confirmed by comparing its XRD pattern with that of pure HPA (Fig. 1). In contrast, impregnation of silica with less bulky triflic acid caused only a slight decrease of the silica surface area, from 272 to 245 m^2/g.

On the other hand, we investigated the presence of triflic acid on TFAS sample by monitoring the IR SO_2^{2-} vibration band at 1417 cm^{-1}, which is regarded as the characteristic band of supported TFA [11]. In Fig. 2 we compare the FTIR spectra of TFAS sample and pure SiO_2. Clearly, addition of TFA to SiO_2 gave rise to a new IR band at 1417 cm^{-1} arising from the stretching of the SO_2 group. The formation of a broad absorption band at 3495 cm^{-1}, attributed to hydrogen-bonded TFA species to the silanols groups of SiO_2, and the consequent intensity decrease of the silanol group band (3734 cm^{-1}) were also observed [11].

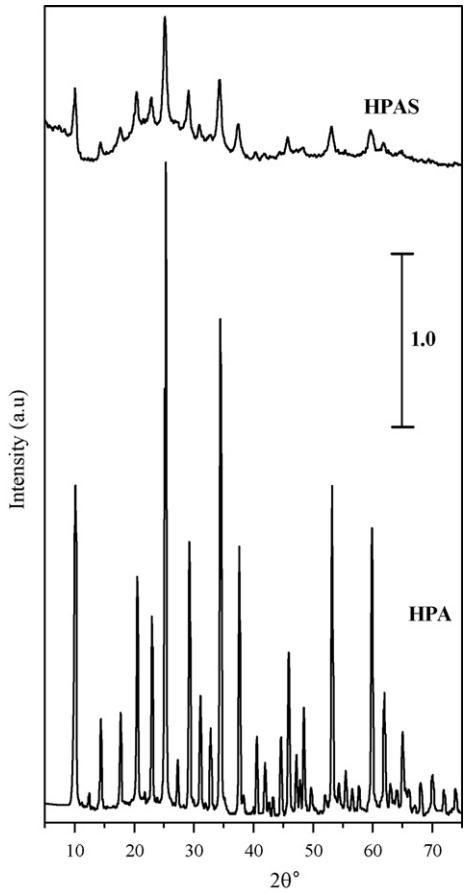

Fig. 1. XRD patterns of HPA and HPAS samples.

We determined the catalyst acid properties by combining TPD of NH_3 and IR spectroscopy of adsorbed pyridine. However, the low stability of triflic acid (the boiling point of TFA is 435 K) hindered the characterization of TFAS sample by TPD of NH_3. On the other hand, resin Amberlyst 35W could not be characterized either by TPD of NH_3 or FTIR of adsorbed pyridine due to its low thermostability. Fig. 3 shows the NH_3 TPD curve obtained on HPAS sample. The NH_3 desorption gave rise to several desorption peaks at temperatures in the range of 500–900 K reflecting the presence of surface acid species that bind NH_3 with different strengths. The total surface acid site density, n_a, was obtained by deconvolution and integration of the NH_3 TPD curve and is presented in Table 1. The proton content (n_{H+}, μmol H+/g cat) measured on HPAS by UV spectroscopy (Table 1, column 4) was similar to the corresponding n_a value (μmol NH_3/g cat). This agreement between n_a and n_{H+} values strongly suggests that the HPA protons are completely accessible for NH_3 adsorption in HPAS sample.

The chemical nature and strength of surface acid sites of HPAS and TFAS were determined from the IR spectra of adsorbed pyridine after admission at 298 K and sequential evacuation at increasing temperatures. The FTIR spectra of adsorbed pyridine after evacuation at 373, 423 and 473 K on HPAS, and at 353 K on TFAS sample are shown in Fig. 4a and b, respectively. TFAS and HPAS catalysts showed the IR bands typical of pyridinium ion formed on Brønsted acid sites, i.e. the ring vibrations modes at 1636, 1608, 1537 and 1485 cm^{-1}, and an additional weak band arising from pyridine coordinated on Lewis acid sites at

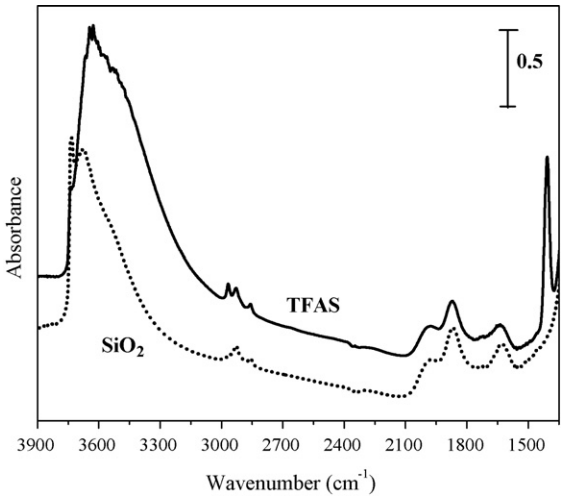

Fig. 2. FTIR spectra of the SiO_2 support after evacuation at 423 K, and of silica-supported triflic acid (TFAS) catalyst after evacuation at 353 K.

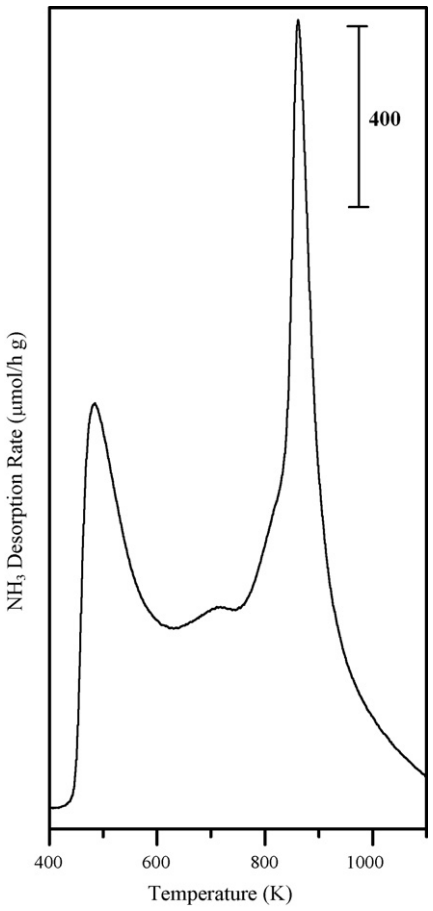

Fig. 3. TPD profile of NH_3 on HPAS sample. NH_3 adsorption at 373, 10 K/min heating rate.

~1450 cm^{-1} [12]. The fact that the HPAS sample displayed both Brønsted and Lewis acid bands suggests that upon impregnation of HPA on SiO_2, in addition to the Keggin structure that accounts for the Brønsted acid species, the heteropolyacid partially transforms giving rise to lacunary or unsaturated species [13] of Lewis acid character formed by interaction with the silica support. A measure of the relative contribution of the Brønsted and Lewis acid sites on HPAS and TFAS samples was obtained from Fig. 4a and b, by integration of the bands at ~1540 and ~1450 cm^{-1}, respectively, corresponding to the 19b ring vibrations of pyridine [14]; results are presented in Table 1. Calculations show that Brønsted acid sites represent about 90% of the total acid density on both samples (Table 1, column 7). Moreover, we observed that the Brønsted/Lewis acid site ratio on HPAS increased with the evacuation temperature, thereby indicating that Brønsted acid sites are more strongly acidic than the Lewis acid sites and retain pyridine up to higher evacuation temperatures. In summary, characterization using IR of adsorbed pyridine shows that HPAS and TFAS samples are essentially solid Brønsted acid catalysts.

3.2. Catalytic testing

3.2.1. Catalyst activity and selectivity

Fig. 5 shows the evolution of ionone yields with reaction time obtained on HPAS, TFAS and Amberlyst 35W samples at 353 K. The local slopes of the ionone yield curves in Fig. 5 give the rate of formation of each product at a specific PS conversion and reaction time. From the curves of Fig. 5 we determined the initial ionone formation rate (r^0_{IONONE}, mmol/h g) by calculating the initial slopes according to:

$$r^0_{IONONE} = \frac{n^0_{PS}}{W}\left[\frac{d\eta_{IONONE}}{dt}\right]_{t=0}$$

where W is the catalyst load and n^0_{PS} is the initial molar amount of PS. The obtained r^0_{IONONE} values are given in Table 2. It is observed that r^0_{IONONE} on TFAS was about twice as high as on Amberlyst 35W and HPAS. Moreover, if the r^0_{IONONE} values obtained on TFAS and

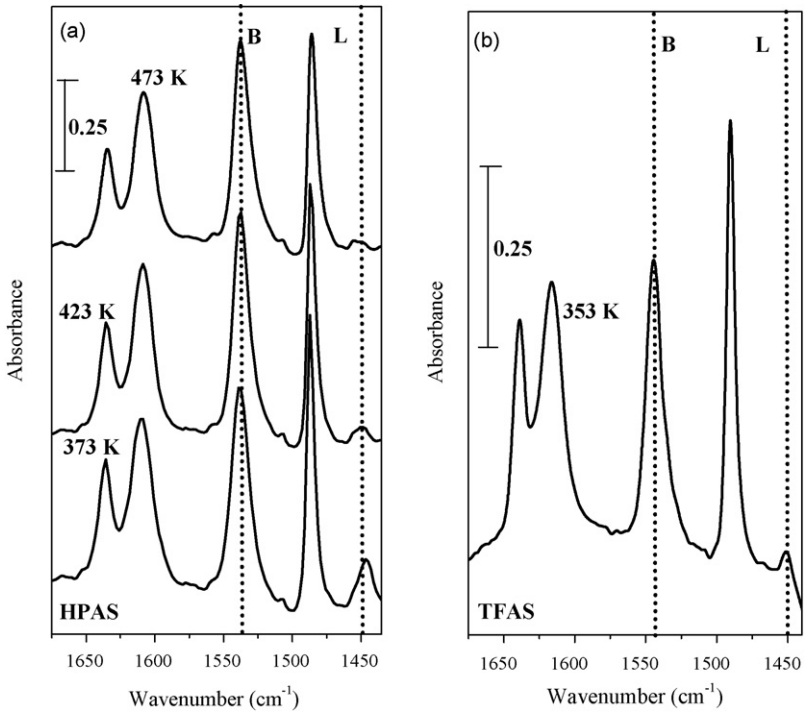

Fig. 4. FTIR spectra of pyridine after adsorption at 298 K and evacuation at (a) 373, 423 and 473 K on HPAS and (b) at 353 K on TFAS. *B*: Brønsted; *L*: Lewis.

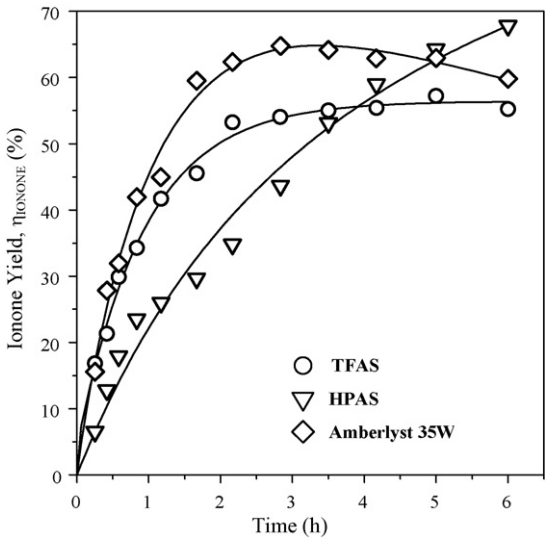

Fig. 5. Ionone yield (η_{IONONE}) as a function of time on HPAS, TFAS and Amberlyst 35W catalysts [T = 353 K, $n^0_{PS} = 0.009$ mol, toluene/PS = 71 (molar ratio), $W_{HPAS} = W_{Amberlyst\ 35W}$ = 1.0 g, W_{TFAS} = 0.5 g].

HPAS are determined per gram of acid loading, then the initial ionone formation rate on TFAS results about 18 times higher in comparison to HPAS. Results in Table 2 reveal that the initial activity order for obtaining ionones is: TFAS > Amberlyst 35W ≈ HPAS. This activity order probably reflects more differences in the catalyst proton site strength than in the catalyst acid site density. In effect, protons on TFA present the strongest acidity on a Hammett acidity function basis ($H_0 = -14.6$) [15], in contrast to −13.2 [16] on HPAS and −2.65 [17] on Amberlyst 35W.

The PS conversion and ionone isomer yields (η_i, i: α-ionone, β-ionone or γ-ionone) as a function of time for HPAS, TFAS, and Amberlyst 35W at 353 K are presented in Fig. 6. The nonzero initial slopes of the isomer yield curves indicate that the three ionones are primary products, i.e. they are formed directly from PS. From the initial slopes of the ionone isomer yield vs. time curves of Fig. 6 we determined the initial formation rate of ionone isomers. Results are shown in Table 2.

The three catalysts converted initially PS mainly to α- and γ-ionones; the r^0_α and r^0_γ values were, effectively, 2–3 times higher in all the cases than those of r^0_β. But the initial ionone isomer distribution was similar on all samples of Table 1, giving an initial α:β:γ isomer ratio of approximately 40:20:40 (Table 2). This result suggests that the initial ionone isomer distribution does not depend on the Brønsted acid site strength.

Fig. 6 also shows that the α-isomer yield curve monotonically grew with reaction time on the three catalysts. In contrast, the γ isomer yield curve reached a maximum at about 80–90% PS conversion on TFAS and Amberlyst 35W, thereby suggesting that on these catalysts γ-ionone is consecutively converted to the other isomers. More insight on the ionone isomer distribution changes with the progress of the reaction is inferred from Fig. 7. In fact,

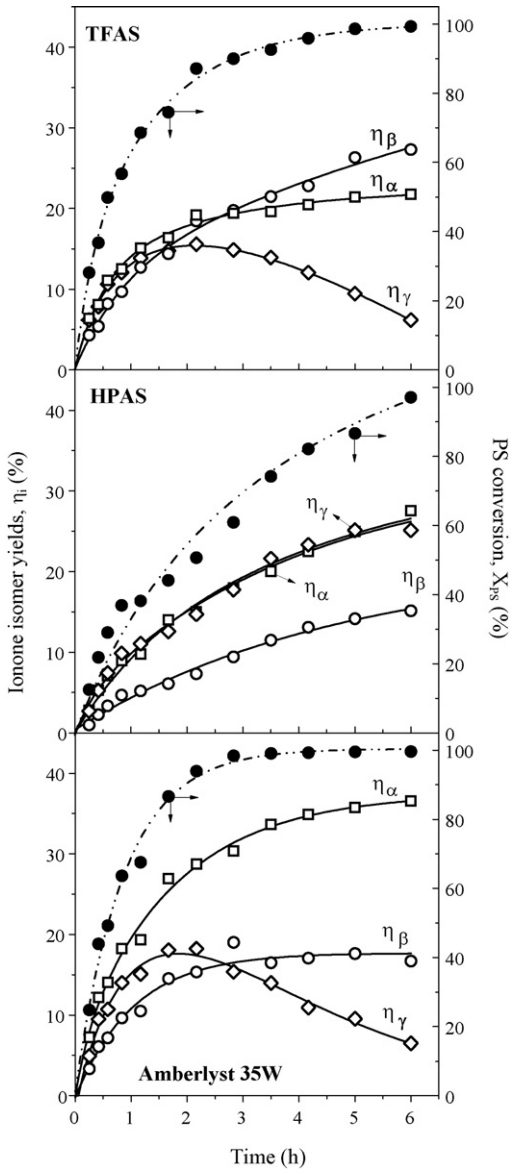

Fig. 6. Ionone isomer yields (η_{IONONE}) and PS conversion as a function of time on HPAS, TFAS and Amberlyst 35W catalysts. Reaction conditions as in Fig. 4.

Fig. 7 shows that on TFAS sample the contribution of β-ionone continuously increased with reaction time at the expenses of γ-ionone attaining ≈50% at the end of the run, while the concentration of α-ionone in the ionone mixture remained almost constant (38%). In contrast, on Amberlyst 35W γ-ionone was converted to α-ionone so that the contribution of α-ionone in the ionone mixture increased from 41% at the beginning of the reaction to 61% at the end of the 6-h run whereas the contribution of β-ionone slightly increased. Finally, although on HPAS the ionone isomer distribution did not change significantly during the 6-h run,

Table 2
Catalytic results on HPAS, TFAS and Amberlyst 35W catalysts.

Catalyst	Initial ionone formation rate (mmol/h g)				Initial ionone isomer distribution (%)		
	r^0_{IONONE}	r^0_α	r^0_β	r^0_γ	α	β	γ
TFAS	11.56	4.56	2.57	4.43	36.2	24.8	39.0
Amberlyst 35W	6.61	3.02	1.38	2.21	40.7	22.0	37.3
HPAS	4.48	1.98	0.60	1.90	38.2	18.9	42.9

Reaction conditions: T = 353 K, P = 250 kPa, $n^0_{PS} = 0.009$ mol, toluene/PS = 71 (molar ratio), $W_{HPAS} = W_{Amberlyst\ 35W}$ = 1.0 g, W_{TFAS} = 0.5 g.

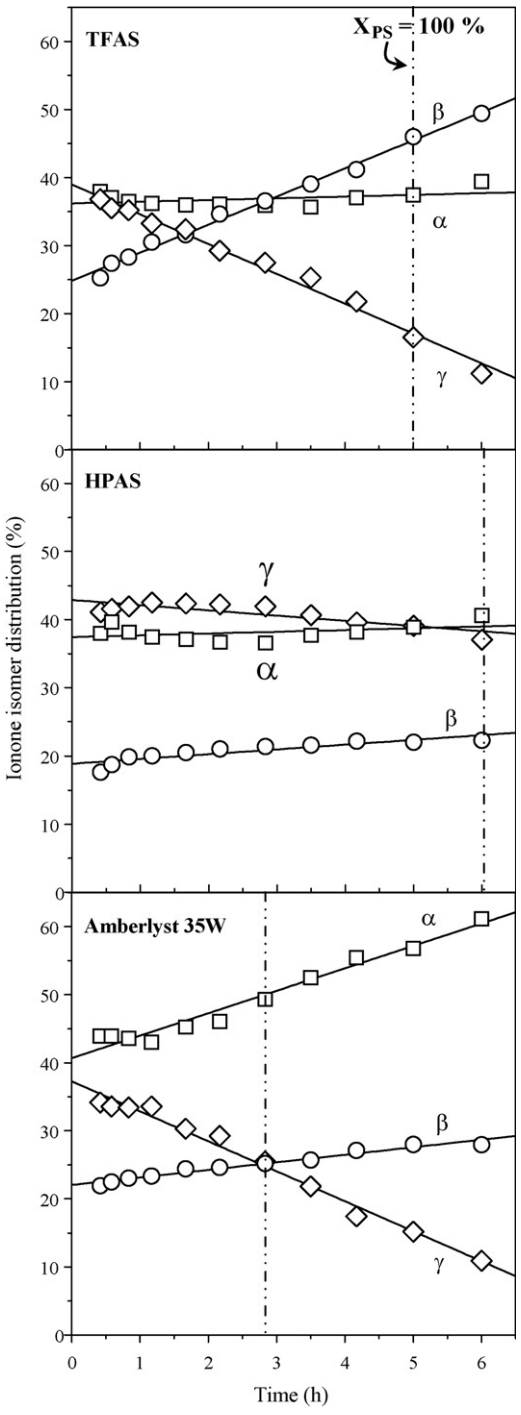

Fig. 7. Ionone isomer distribution as a function of time on HPAS, TFAS and Amberlyst 35W catalysts. Dotted line: reaction time at 100% PS conversion. Reaction conditions as in Fig. 4.

some isomer interconversion can be observed. In summary, results of Figs. 6 and 7 show that the kinetics of ionone isomer interconversion is affected by the catalyst surface proton strength.

To explore the effect of temperature on catalyst activity and selectivity, we performed additional catalytic tests on sample HPAS varying the reaction temperature between 343 and 383 K. Specifically, we carried out catalytic tests at 343, 353, 363, 373, and 383 K. Fig. 8 illustrates the results obtained at 383 K. At this temperature, PS was completely converted in 2 h. The contribution of α-ionone continuously grew at the expense of the γ-isomer with the progress of the reaction, while the contribution of the β-isomer

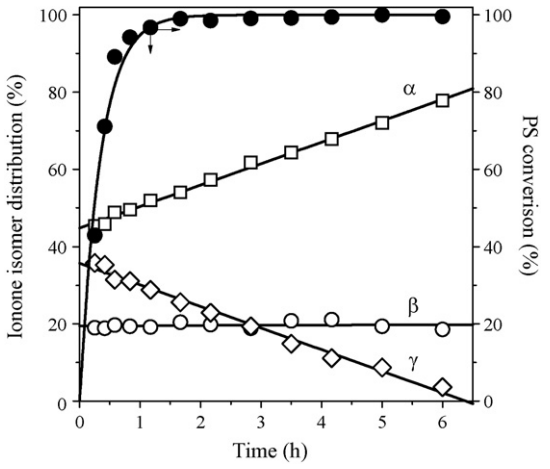

Fig. 8. Ionone isomer distribution and PS conversion as a function of time on HPAS sample [T = 383 K, $n^0_{PS} = 0.009$ mol, toluene/PS = 71 (molar ratio), W_{HPAS} = 1.0 g].

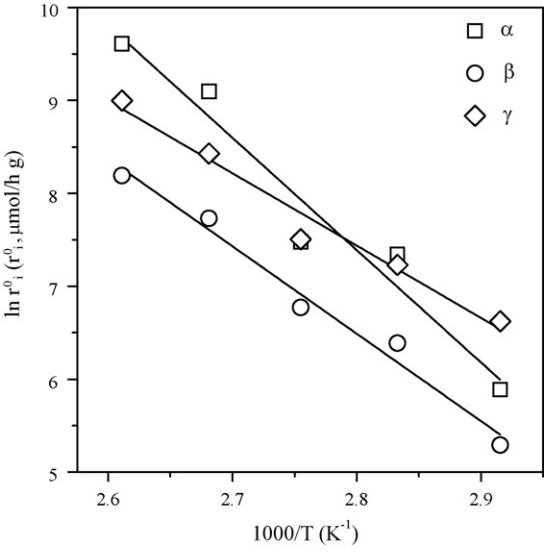

Fig. 9. Arrhenius plots for the formation of α-, β- and γ-ionones from pseudoionone on HPAS [T = 343–383 K, $n^0_{PS} = 0.009$ mol, toluene/PS = 71 (molar ratio), W_{HPAS} = 1.0 g].

remained almost constant. This qualitative evolution of ionone isomer distribution with reaction time is similar to that observed on Amberlyst 35W at 353 K in Fig. 7.

From the ionone isomer yields vs. time curves obtained on HPAS at 343, 353, 363, 373 and 383 K, we determined first the initial formation rates and then the apparent activation energy, E_a, for each individual ionone isomer. The apparent activation energies for the formation of ionone isomers were determined using an Arrhenius-type function ($r^0_i = Ae^{-E_a/RT}$, where A is a constant containing the pre-exponential factor) by plotting $\ln r^0_i$ values as a function of 1000/T, Fig. 9. The E_a values obtained for the synthesis of α-, β- and γ-ionones from PS were 24, 19 and 15 kcal/mol, respectively. These values indicate that an increase in reaction temperature on HPAS would promote more the formation of α-ionone than β- and γ-ionones in agreement with our experimental results. For example, the initial contribution of the α-isomer in the ionone mixture on HPAS increased from 38.2% at 353 K to 44.8% at 383 K, while for the same temperatures γ-ionone decreased from 42.9 to 35.7%.

The calculated kinetic parameters A and E_a for the formation of the three ionone isomers were plotted in Fig. 10 as $\ln A$ vs. E_a in

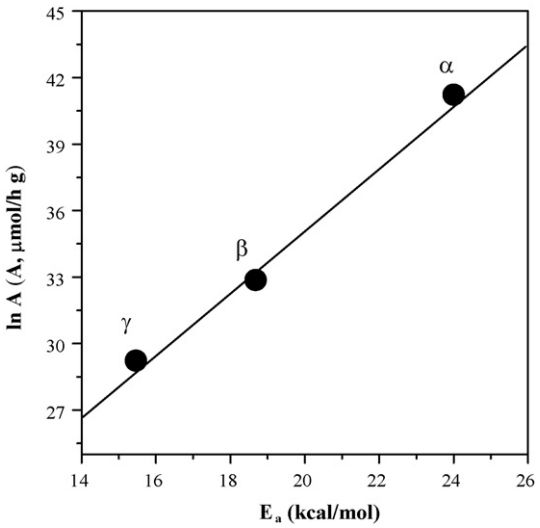

Fig. 10. Compensation effect in ionone isomer formation on HPAS.

order to determine if the experimental data obey a Cremer–Constable relation [18,19]

$$\ln A = mE_a + c$$

The resulting linear correlation in this semilogarithmic plot is indicative of the existence of a "Compensation Effect" in the kinetics of ionone isomer formation on HPAS.

3.2.2. Reaction mechanism

The reaction pathways of PS cyclization to ionone isomers have been studied almost exclusively using liquid acid catalysts. Royals [20] investigated the cyclization of PS using different liquid acids such as H_2SO_4, H_3PO_4, Cl_3CCOOH, and $ClCH_2COOH$. They observed that the composition of the ionone mixture depends on the acid strength. In fact, the proportion of β-ionone increased with the strength of the acid while formation of α-ionone was predominant when using weakly acidic media. Consistently, other authors have reported that concentrated sulfuric acid produces mainly β-ionone [8,9]. Markovich et al. [21,22] studied the synthesis of β-ionone using trifluoroacetic acid, fluorosulfonic acid and anhydrous hydrogen fluoride. They postulated that medium strength liquid acids promote the PS protonation forming an enol carbonium that leads to α-ionone by rearrangement. Consecutively, strong liquid acids may protonate the cyclic double bond of α-ionone forming a carbonium ion that leads to the formation of β-ionone. Other authors [3] noted that medium strength liquid acids such as phosphoric acid form essentially α-ionone.

Based on the results of Figs. 6–8, we present in Scheme 2 the reaction pathways involved in the synthesis of ionone isomers from PS on HPAS, TFAS and Amberlyst 35W catalysts. We postulate that the PS molecule is initially activated on surface Brønsted acid sites and forms a common cyclic intermediate for the consecutive ionone isomer formation. The synthesis of the three ionone isomers from PS via the same cyclic carbocation intermediate is consistent with the compensation effect observed for the initial formation of ionone isomers on HPAS sample (Fig. 10). As noted previously [23–25], the compensation effect is frequently verified when a catalyst promotes a group of reactions involving compounds of analogous molecular structures, sharing the same mechanism and transition state. The common cyclic intermediate in Scheme 2 contains H_α (two), H_β (one) and H_γ (three) protons that have to be detached to form α-, β- and γ-ionone, respectively. We observed here (Fig. 6) that the three ionone isomers are formed directly from PS, i.e. they are primary products.

On the other hand, our results on the initial ionone isomer formation rates in Table 2, show that on TFAS, HPAS and Amberlyst 35W samples the PS conversion forms initially ionone mixtures of similar composition, containing about 40% α-ionone, 20% β-ionone and 40% γ-ionone, which is close to the statistical composition (α:β:γ = 33:17:50). This result strongly suggests that the initial selectivity of ionone isomers does not depend significantly on the strength of surface Brønsted acid sites. In contrast, the ionone isomer interconversion during the progress of the reaction depended on the acid site strength. In fact, γ-ionone was isomerized to α-ionone on HPAS and Amberlyst 35W (Figs. 7 and 8), while the stronger acid sites of TFAS converted γ-ionone to β-ionone (Fig. 7).

Analyzing the chemical structure of the ionone molecules (Scheme 1), it can be assumed the following stability order: β > α > γ-ionone. The β-isomer is highly stable due to the molecule extended conjugated system and therefore is not isomerized to α- or γ-ionones. In contrast, taking into account

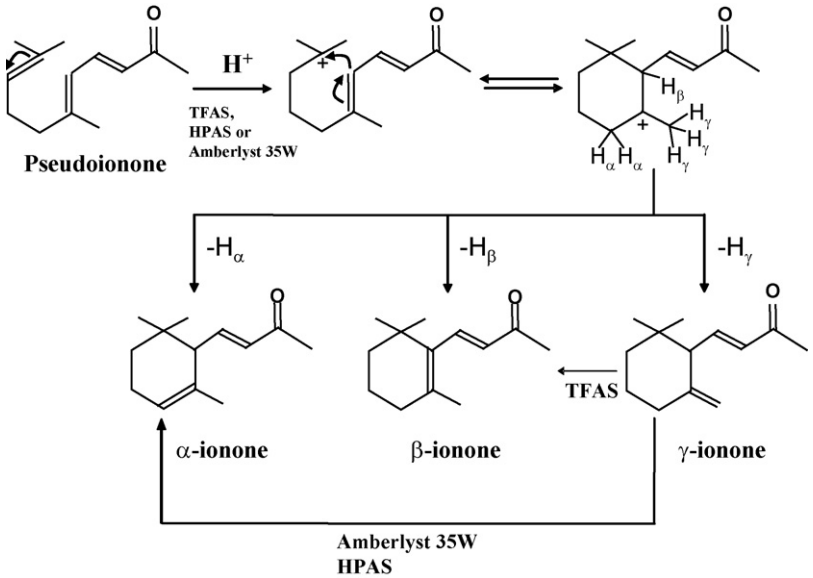

Scheme 2. Reaction network for the synthesis of ionone isomers from pseudoionone on Brønsted acid catalysts.

the instability and reactivity of γ-ionone because of the exocyclic C=C bond in this molecule, conversion to the other ionones with the progress of the reaction is expected.

In summary, our results show that the ionone isomer mixture composition can be controlled by changing the Brønsted acid site strength, temperature and reaction time. The initial PS conversion forms ionone mixtures with nearly statistical composition, irrespective of the Brønsted acid site strength. By increasing the temperature and/or the reaction time, γ-ionone is transformed to α- or β-ionone, depending on the Brønsted acid site strength. Final ionone mixtures containing essentially α- and β-ionone may be obtained at 353 K on TFAS (mixture of about 50% β-ionone and 40% α-ionone) and on Amberlyst 35W (mixture of about 60% α-ionone and 30% β-ionone) or at 383 K on HPAS (mixture of about 80% α-ionone and 20% β-ionone).

4. Conclusions

The liquid-phase synthesis of ionone isomers (α-, β- and γ-ionone) from pseudoionone cyclization is efficiently achieved on solid Brønsted acid catalysts such as Amberlyst 35W, silica-supported triflic acid (TFAS) and silica-supported heteropolyacid (HPAS). Catalyst activity depends on the surface acid site strength so that the initial activity order for obtaining ionones is TFAS > Amberlyst 35W ≈HPAS.

The pseudoionone molecule is initially activated on surface Brønsted acid sites and forms a common cyclic intermediate for the consecutive ionone isomer generation. This cyclic carbocation intermediate contains three different kinds of protons that upon direct detachment lead to α-, β- or γ-ionones as primary products.

Selectivity to the three ionone isomers is also strongly dependent on the acid site strength. Under initial conditions, pseudoionone transformation gives ionone mixtures with approximately statistical composition (40% α-ionone, 20% β-ionone and 40% γ-ionone), regardless of the catalyst Brønsted acid site strength. However, with the progress of the reaction γ-ionone, the least stable isomer, is isomerized to α-ionone on HPAS and Amberlyst 35W, and to β-ionone on the stronger acid sites of TFAS.

Therefore, binary mixtures of α- and β-ionone can be obtained by properly selecting operational conditions since the kinetics of ionone isomer interconversion may be controlled by changing the Brønsted acid site strength, temperature and reaction time.

Acknowledgements

Authors thank the Agencia Nacional de Promoción Científica y Tecnológica (ANPCyT), Argentina (Grant PICT 14-11093/02), CONICET, Argentina (Grant PIP 5168/05) and the Universidad Nacional del Litoral, Santa Fe, Argentina (Grant CAI+D 007-040/05) for the financial support of this work. They also thank H. Cabral for technical assistance.

References

[1] Ullmann's Encyclopedia of Industrial Chemistry, 6th ed., 2002 (electronic).
[2] E. Brenna, C. Fuganti, S. Serra, P. Kraft, Eur. J. Org. Chem. (2002) 967.
[3] H. Hibbert, L.T. Cannon, J. Am. Chem. Soc. 46 (1924) 119.
[4] Z. Lin, H. Ni, H. Du, C. Zhao, Catal. Commun. 8 (2007) 31.
[5] D. Guo, Z.-F. Ma, Q.-Z. Jiang, H.-H. Xu, Z.-F. Ma, W.-D. Ye, Catal. Lett. 107 (2006) 155.
[6] V.K. Díez, C.R. Apesteguía, J.I. Di Cosimo, Catal. Lett. 123 (2008) 213.
[7] V.K. Díez, B.J. Marcos, C.R. Apesteguía, J.I. Di Cosimo, Appl. Catal. A: Gen. 358 (2009) 95.
[8] K. Steiner, H. Ertel, H. Tiltscher, US Patent 5,453,546, to Hoffmann-La Roche Inc. (1995).
[9] U. Rheude, U. Horcher, D. Weller, M. Stroezel, US Patent 6,288,282, to BASF Aktiengesellschaft (2001).
[10] G. Ohloff, G. Schade, Angew. Chem. Int. Ed. 2 (1963) 149.
[11] A. de Angelis, C. Flego, P. Ingallina, L. Montanari, M.G. Clerici, C. Carati, C. Perego, Catal. Today 65 (2001) 363.
[12] C. Morterra, A. Chiorino, G. Ghiotti, E. Fisicaro, J. Chem. Soc. Faraday Trans. I 78 (1982) 2649.
[13] I.V. Kozhevnikov, K.R. Kloetstra, A. Sinnema, H.W. Zandbergen, H. van Bekkum, J. Mol. Catal. A: Chem. 114 (1996) 287.
[14] B. Bachiller-Baeza, J.A. Anderson, J. Catal. 228 (2004) 225.
[15] C.K. Jørgensen, Naturwissenschaften 67 (1980) 188.
[16] T. Okuhara, M. Misono, in: R.B. King (Ed.), Encyclopedia of Organic Chemistry, John Wiley and Sons, 1994.
[17] R. Bringué, M. Iborra, J. Tejero, J.F. Izquierdo, F. Cunill, C. Fité, V.J. Cruz, J. Catal. 244 (2006) 33.
[18] F.H. Constable, Proc. Roy. Soc. (London) 108 (1925) 355.
[19] E. Cremer, Z. Phys. Chem. 144 (1929) 231.
[20] E.E. Royals, Ind. Eng. Chem. 38 (1946) 546.
[21] Y.D. Markovich, A.V. Panfilov, A.A. Zhirov, A.T. Kirsanov, L.A. Gorbach, K.A. Taraskin, Pharm. Chem. J. 32 (10) (1998) 557.
[22] Y.D. Markovich, A.V. Panfilov, Y.N. Platunov, A.A. Zhirov, S.I. Kosenko, A.T. Kirsanov, Pharm. Chem. J. 32 (11) (1998) 603.
[23] G.C. Bond, M.A. Keane, H. Kral, J.A. Lercher, Catal. Rev. Sci. Eng. 42 (3) (2000) 323.
[24] M. Boudart, Chem. Eng. Prog. 57 (1961) 33.
[25] A.K. Galwey, Adv. Catal. 26 (1977) 247.